SYNTHESIS OF ZEOLITE SUPPORTED Cu_2O-Ag_3PO_4-ZnO NANOCOMPOSITE FOR PHTOCATALYTIC DEGRADATION OF METYLENE BLUE UNDER VISIBLE LIGHT

MSC GRADUATE PROJECT

MESFIN G/EGZIABHER G/SILASSIE

MARCH 2018

HARAMAYA UNIVERSITY, HARAMAYA

Synthesis of Zeolite Supported Cu_2O-Ag_3PO_4-ZnO Nanocomposite for Phtocatalytic Degradation of Methylene Blue Under Visible Light

MSc Graduate Project Submitted to the Department of Chemistry, Postgraduat Program

Directorate

Haramaya University

In Partial Fulfillment of the Requirements for the Degree of

Master of Science in Chemistry (Physical)

Mesfin G/Egziabher G/Silassie

March 2018

Haramaya University, Haramaya

HARAMAYA UNIVERSITY

POST GRADUATE PROGRAME DIRECTORATE

I hereby certify that I have read and evaluated this **MSc Graduate Project** entitled **''Synthesis of Zeolite Supported Cu_2O-Ag_3PO_4-ZnO Nanocomposite and Phtocatalytic Degradation of Methylene Blue under Visible Light"** prepared under my guidance by **Mesfin G/Egziabher.** I recommend that it be submitted as fulfilling the **MSc Graduat Project** requirement.

Abi Taddesse (PhD) _____ _____

Major Advisor Signature Date

As a member of the Board of Examiners of the MSc Thesis Open Defense Examination, I certify that I have read and evaluated the Thesis prepared by **Mesfin G/Egziabher** and examined the candidate. I recommend that the **MSc Graduate Project** be accepted as fulfilling the Thesis requirement for the degree of **Master of Science in Chemistry (Physical Chemistry)**.

_____ _____ _____

Chairperson Signature Date

_____ _____ _____

Internal Examiner Signature Date

_____ _____ _____

External Examiner Signature Date

DEDICATION

To my beloved Zelalem Engida and to my parents, for standing by my side in the successful accomplishment of this work.

STATEMENT OF THE AUTHOR

By my signature below, I declare and affirm that this **MSc Graduate Project** is my own work. I have followed all ethical and technical principles of scholarship in the preparation, data collection, data analysis and compilation of this Research. Any Scholarity matter that is included in the research has been given recognition through citation.

This research has been submitted in partial fulfillment of the requirements for a MSc degree at Haramaya University. The Research is deposited in the Haramaya University library and is made available to borrowers under rules of the library. I solemnly declare that this Research has not been submitted to any other institution anywhere for the award of any academic degree, diploma, or certificate.

Brief quotations from this Research possible without special permission provided that accurate and complete acknowledgement of source is made. Requests for permission for extended quotation from or reproduction of this research in whole or in part may be granted by the head of the Department or the Director of the Postgraduate Program Directorate when in his or her judgment the proposed use of the material is in the interests of scholarship. In all other instances, however, permission must be obtained from the author of the Rsearch.

Name: **Mesfin G/Egziabher** Signature: _____

Date of Submission: _____

School/Department: _____

BIOGRAPHICAL SKETCH

The author, **Mesfin G/Egziabher** was born April 03, 1973 E.C in Assela city which is in Oromia Regional Administration. He attended his elementary and secondary school education at Assela Primary and secondary School. After completion of his secondary school education, he joined Adama College Teachers Training Education in 1992 E.C. After graduation, he was employed by South Region Education Bureau as a teacher in Yirgalem Secondary and preparatory School and then graduated with BED in Chemistry from Haramaya University in 2000 E.C. Three years later, he joined the School of Graduate Studies of Haramaya University in 2004 E.C summer program to pursue master program in chemistry (Physical Chemistry) as self-sponsored student.

ACKNOWLEDGEMENTS

I would like to express my deepest gratitude and heartfelt thanks to my advisor, Dr. Abi Taddesse, for his guidance and encouragement on every stage of this research work, including the conception of the topic, constructive advice, useful discussion, continuous guidance, friendly treatment, encouragement, visits to my laboratory work and correcting this thesis.

Next, I would like to give special thanks to staffs of Chemistry Department of Haramaya University and laboratory technicians for providing me the necessary information, introducing the laboratory facilities and technical supports.

My special thanks also go to my family: my wife sister Zelalem Engida and our children Arsemawit and Natinel Mesfin they provided me consistent encouragement, company, laughter, a listening ear and much more over the years and along the way, both in person and over the phone. I am grateful to them all for taking their parental roles. I was hosted, fed, loved and allowed to be member of the family. From this family, I received much more than I can possibly say. They represent a crucial part of my academic performance, even beyond helping me in this particular project and I remember them with much affection and gratitude.

I am also grateful to Addis Ababa University, Institute of technology, for their cooperation in running the Nitrogen Bergen Furnace and Adama university for XRD analyses.

ACRYNOYMS AND ABRIVATIONS

Eg	Band gap Energy
BET	Brunauer- Emmett- Teller
CB	Conduction Band
FT-IR	Foruier- Transformed Infrared Spectroscopy
GSE	Geological Survey of Ethiopia
MO-NPS	Metal oxide nanoparticle
MB	Methylene blue
SEM	Scanning Electron Microscope
VB	Valence Band
XRD	X- Ray Diffractometer
NCS	Nanocomposite
Z-5O% NCS	50% Zeolite supported NCS

TABLE OF CONTENT

DEDICATION	iv
STATEMENT OF THE AUTHOR	v
BIOGRAPHICAL SKETCH	vi
ACKNOWLEDGEMENTS	vii
ACRYNOYMS AND ABRIVATIONS	viii
TABLE OF CONTENT	ix
TABLE OF FIGURES	xi
ABSTRACT	xiii
1. INTRODUCTION	1
1.2. Objective of the Study	4
1.2.1. General Objective of the Study	4
1.2.2. Specific Objectives	4
2. REVIEW LITERATURE	5
2.1. Photocatalysis	5
2.1.1. Basic Principles and Mechanism of Photocatalysis	5
2.1.2. Photocatalytic Degradation	8
2.1.3. Determining the Rate Law from Experimental Data	9
2.1.4. Zeolite as a Supporte for Nanomaterial	9
2.2. Factors Affecting Photocatalytic Degradation of Dye	10
2.2.1. Dye Type and pH Effect	10
2.2.2. Effect of Photocatalyst Load Under Visible Light	12
2.2.3. Effect of Initial Concentration of Dye	13
2.2.4. Effect of Temperature	13
2.3. Degradation Mechanism of Methylene Blue	13
2.4. Method to Synthesis Nanomaterials	15
2.4.1. Co- Precipitation Method	15
2.4.2. Top Down and Bottom up Synthesis	16
2.4.3. Sol–gel Processing	16
2.4.4. Hydrothermal Method	17
2.5. Characterization of Photocatalyst Nanoparticles	18

2.5. 1. X-ray Diffraction Method 18
2.5. 2. UV-Visible Absorption Method 19
2.5.3. TEM/SEM Microscope 19
2.5.4. Fourier-Transformed Infrared Spectroscopy (FT-IR) Method 19
3. MATERIALS AND METHODS 21
3.1. Experimental Site 21
3.2. Apparatus and Equipments 21
3.3. Methods and Procedures 21
3.3.1. Synthesis of Cu_2O-Ag_3PO_4-ZnO Ternary Composite 21
3.3.2. Preparation of Zeolite Supported Cu_2O-Ag_3PO_4-ZnO Nanocomposite. 22
3.4. Characterization of Photocatalysts 22
3.4.1. XRD Method 22
3.4.2. Uv/vis Spectrophotometer Method 23
3.5. Kinetic Study of Photocatalytic Degradation 23
4. RESULT AND DISCUSION 24
4.1. Characterization of the As-Synthesized Nanocomposite 24
4.1.1. XRD Analysis 24
4.2. Photocatalytic Studies Cu_2O-Ag_3PO_4-ZnO Ternary Composite 26
4.2.1. Comparison of Photocatalytic Activities of the As-synthesized Photocatalysts 26
4.2.2. Effect of Initial Dye Concentration 27
4.2.3. Effect of Zeolite on Photocatalytic Degradation 29
4.2.4. Kinetic Study of Methylene Blue Degradation 30
5. SUMMARY AND CONCLUSIONS 34
6. REFERENCES 35
7. APENDICS 433

LIST OF FIGURES

Figure Page

1. Electrons transfer from CB of Cu_2O generated by visual light can transfer to the CB of ZnO. 6

2. Electrons transfer from ZnO to Ag_3PO_4 7

3. The formation of Ag_3PO_4/ZnO composite heterostructure 8

4. Structure of methylene blue 11

5. Decolorization of methylene blue dye in presence of Cu_2O NPs. 11

6: XRD Plot for Sample with unsupported (NCS) and supported (Z_50) 25

7. Efect of time on photo degradation of MB using supported and unsupported photocatalysts: MB = 10 mg/L , catalyst load =120 mg/L. 27

8. Plots of % degradation of MB as function of time under visible light irradiation by keeping the unsupported photocatalyst load constant(10mg/l) and varying the amount of MB solution. 28

9. Plots of % degradation of MB as function of time under visible light irradiation by keeping the supported photocatalyst load constant(120mg/l) and varying the amount of MB solution. 29

10. The corresponding comparison of different concentration of MB photodegradation under visible light irradiation Unsupported Ncs. 31

11. Kinetic study of ln(Co/Ct) as a function of time for MB degradation at different initial dye concentration of unsupported Ncs. 32

LIST OF TABLES IN THE APPENDIX

TABLE **PAGE**

Appendix Table. Data Analysis of unsupported Ncs and zeolite supported Ncs……43

Synthesis of Zeolite Supported Cu_2O-Ag_3PO_4-ZnO Nanocomposite for Phtocatalytic Degradation of Metylene Blue under Visible Light

ABSTRACT

Nano sized Cu_2O-Ag_3PO_4-ZnO nanocomposite was prepared by precipitation method using different salt solution and solid state reaction of the as-synthesized nanocomposite with natural zeolite to produce zeolite supported Cu_2O-Ag_3PO_4-ZnO fine particles. The structure of the composites was studied using X-ray diffraction (XRD). The result show that the average crystalline sizes of unsupported and supported nanocmposite become 46.63nm and 50.85nm respectively recorded. The rate of decolorization of organic dyes increases as the particle size decreases. This is because of increase in the specific surface area of a photocatalyst as the crystalline dimension decrease. Photocatalytic degradation activities of the nanocomposites under visible light irradiation have been evaluated for a model pollutant methylene blue (MB) dye solution. Natural zeolite supported Cu_2O-Ag_3PO_4-ZnO nanocomposite photocatalyst exhibited a relatively higher efficiency on the photodegradation of methylene blue (MB) to the extent of about 88.2%. The present work suggests on the possible use of natural zeiolite as a support for nanomaterials to enhance the reusability of the photocatalyst material.

Keywords: Copperousoxide(Cu_2O)- Silverphosphate(Ag_3PO_4)- Zincoxide(ZnO) ternary Nanocomposite, Natural zeolites, Methylene blue, Photocatalysis,

1. INTRODUCTION

In recent years, semiconductor photocatalytic process has shown a great potential as a low-cost, environmental friendly and sustainable treatment technology to align with the "zero" waste scheme in the water/wastewater industry. The ability of this advanced oxidation technology has been widely demonstrated to remove persistent organic compounds and microorganisms in water. At present, the main technical barriers that impede its commercialization remained on the post-recovery of the catalyst particles after water treatment. Photocatalysis is of great interest due to the relative ease of the process. The advantage of the process is that it can completely mineralize recalcitrant pollutants into simpler compounds that are benign or can be processed by natural mechanisms to harmless constituents. Moreover, this method does not transfer the pollutant from one phase to another, as in case of certain conventional treatment techniques such as adsorption but rather eliminates the target compound. Photocatalysis has attracted considerable attention attributing to the fact that it provides a new way to meet the challenges of the environment, energy and sustainability (Chen *et al*., 2010). Photocatalysis, apart from pollutant degradation has many other applications. With the development of efficient photocatalytic systems, significant efforts have been devoted to synthesize highly active photocatalysts that function with visible light, and which can be applied in a wide region such as water splitting for hydrogen production, removal and degradation of pollutants and water purification (Kumar *et al*., 2011). Semiconductor oxides, sulphides and halides are commonly employed as photocatalysts. However, it is necessary to note that, most photocatalysis studies are still devoted to archetypical photocatalysts such as TiO_2 and ZnO (Salinaro, 1999). These, semiconductor materials generally act as sensitizers for the light-induced redox reactions that takes place, leading to the mineralisation of the pollutants. Since the photocatalysts are generally based on semiconducting materials, a brief knowledge of semiconductors is essential for the understanding of photocatalytic systems. Clearly, the valence band and conduction band in semiconductors are separated by an energy gap, commonly called as Band gap (Eg).

The biggest use of copper nano powders represents the area of catalysis. Chemical reactions catalyzed by fine powders exhibit faster kinetics and can be often carried out at lower temperatures in comparison to reactions catalyzed by bulk material. Cu_2O is a p-type

semiconductor with a narrow band gap of 2.0 eV and therefore, has been considered to be a potential visible light photocatalyst (Wang *et al*., 2012). The electrons of Cu_2O undergo excitation by visible light and involved in the processes of degradation of dyes in waste water. However, the easy recombination of photo-generated electrons and holes affect its photocatalytic activity. Cu_2O combined with other metal oxides become an effective means to overcome the above weakness of recombination of photo-generated electrons and holes (Zhang *et al.,* 2011).

Recently, Ag_3PO_4 has attracted considerable attention as a potential visible light photocatalyst, and it is a pale yellow semiconductor with a band gap of ca. 2.45 eV. The VB potential of Ag_3PO_4 is lower than that of ZnO with 2.6 eV. The Ag_3PO_4 photocatalyst is unstable under visible light irradiation, and it is easily corroded by the photogenerated electrons (Kikugawa *et al.,* 2010). Furthermore, the unwanted and uncontrolled photodecomposition by light and the low structural stability in water of Ag_3PO_4 decreased the photocatalytic activity during the photocatalytic reaction, which inevitably become a main obstacle for Ag_3PO_4 in practical application (Che *et al.,* 2010).

ZnO has been widely used as a photocatalyst, owing to its high activity, low cost, and environmentally friendly feature (Zhang *et al.,* 2011). However, the photocatalytic activity of ZnO is limited to irradiation wavelengths below 387 nm because ZnO semiconductor has awide band-gap of about 3.2 eV and only 3–5% of the whole solar energy is effectively utilized, while 43% of the visible light is open to exploit.

Cu_2O/ZnO nanocomposite has the best photocatalytic activity compared to pureCu_2O and ZnO. It has been reported that the CB and VB edge of Cu_2O lie above that of ZnO (Helaïli *et al*., 2010), so the electrons in the CB of Cu_2O generated by visual light can transfer to the CB of ZnO. Photodecomposition over semiconductor oxides is initiated by the absorption of a photon with energy equal to or greater than the band gap of semiconductor producing electron–hole pairs. In the ZnO/Cu_2O system, Cu_2O is a sensitizer absorbing visible light and ZnO is used as an acceptor to extract generated electrons. The conduction band position of ZnO is lower than that of Cu_2O (Jiang *et al.,* 2013), so theoretically speaking, the generated electrons in Cu_2O can be transferred to ZnO. The electrons transfer from ZnO to Ag_3PO_4 not

only suppresses the recombination of photogenerated electrons and holes but also facilitates the OH radicals generation in the VB of ZnO, and thus has significant influence on the visible light photocatalytic degradation of the organic dye. But the difficulties in recycling and preconcentration which restricted the utilization of finer nanoparticles. Thus, the nanoparticles have been supposed to be fixed on the inert supports for practical applications in order to improve the recovery efficiency of photocatalysts (Bouzaza *et al.*, 2002).

Ternary nanocomposite having more than one pathway for the formation of electron–hole pair because of the three different interfaces and the electron–hole pair recombination is prevented to the maximum extent in the ternary nanocomposite (Ansari *et al.*, 2013). Kim *et al*, (2011) reported the synthesis of $CdS/TiO_2/WO_3$ ternary hybrid systems as new photoactive composites and found that the ternary hybrid exhibited much higher photocatalytic activity than that of binary hybrids. Although the ternary nanocomposites demonstrated better photocatalytic efficiency compared to single or binary counterparts, they are liable to loss when used naked in a batch or column approach making recovery of these nanomaterials difficult. To circumvent such challenges, one possible approach is to fix or immobilize these nanomaterials to an innert support.

Supporting the nanocomposites on the zeolite increases its adsorption capacity and results in higher concentration of dye molecules around the nanocomposites. On the other hand, good dispersion of the nanocomposites increases the active sites around the adsorbed molecules and the degradation rate of the pollutant becomes faster (Khatamian *et al*., 2012). Furthermore, the strong electrostatic field present in the zeolite framework can effectively separate the electrons and holes produced during photoexcitation of the ZnO and so resulted in lower recombination of them and higher photodegradation efficiency as compared to the naked ternary nanocomposite (Khatamian *et al*., 2012). The natural zeolitized tuffs could serve as a sorbent for the removal of copper, zinc and nickel from aqueous media (Stojakovic *et al.,* 2011). In our laboratory, zeolite supported ternary systems are being prepared for various applications including photocatalysis (Tedla *et al*., 2015; Getachew 2016). Although various ternary nanocomposites are being supported by zeolite, no work has been done on immobilization of $Cu_2O/ZnO/ Ag_3PO_4$ ternary nanocomposite on zeolites for photocatalytic applications. The

aim of this study was therefore to evaluate the photocatalytic degradation of MB by zeolite supported Cu_2O/ZnO/ Ag_3PO_4 ternary nanocomposite under visible light irradiation.

1.2. Objective of the Study

1.2.1. General Objective of the Study

To study photocatalytic activity of zeolite supported Cu_2O/Ag_3PO_4/ZnO nanocomposite for the removal of methylene blue.

1.2.2. Specific Objectives

- To synthesis Cu_2O/Ag_3PO_4/ZnO and Z-Cu_2O/Ag_3PO_4/ZnO ternary nanocomposites by preceptation method.
- To optimize the nanocomposite using XRD and UV-Visible methods.
- To investigate the photocatalytic degradation performance of the nanocomposite towards degradation of MB.

2. REVIEW LITERATURE

2.1. Photocatalysis

In the presence of a photocatalyst, an organic pollutant can be oxidized directly by means of a photogenerated hole or indirectly via a reaction with characteristic reactive groups, for example the hydroxyl radical, produced in solution (Jain *et al.,* 2014). Semiconductor materials generally act as sensitizers for the light-induced redox reactions that take place, leading to the mineralisation of the pollutants. Since the photocatalysts are generally based on semiconducting materials, a brief knowledge of semiconductors is essential for the understanding of photocatalytic systems.

2.1.1. Basic Principles and Mechanism of Photocatalysis

A nanophotocatalyst when exposed to light valance band electrons absorb energy and transfer to conduction band producing an electron-hole pair. The hole in VB reacts with H_2O to give •OH and electron in CB react with dissolved O_2 to give $^{-}O_2$ (Mahmoodi *et al*., 2006). These active radicals are responsible to decompose dye. Ag_3PO_4 photocatalyst is unstable under visible light irradiation, and it is easily corroded by the photogenerated electrons (Kikugawa *et al*.,2010). Furthermore, the unwanted and uncontrolled photodecomposition by light and the low structural stability in water of Ag_3PO_4 decreased the photocatalytic activity during the photocatalytic reaction, which inevitably become a main obstacle for Ag_3PO_4 in practical application (Che *et al* .,2012).

The conduction band (CB) and valence band (VB) edge of Cu_2O lie above that of ZnO (Helaïli *et al.,*2010), so the electrons in the CB of Cu_2O generated by visual light can transfer to the CB of ZnO. In the ZnO–Cu_2O system, Cu_2O is a sensitizer absorbing visible light and ZnO is used as an acceptor to extract generated electrons.

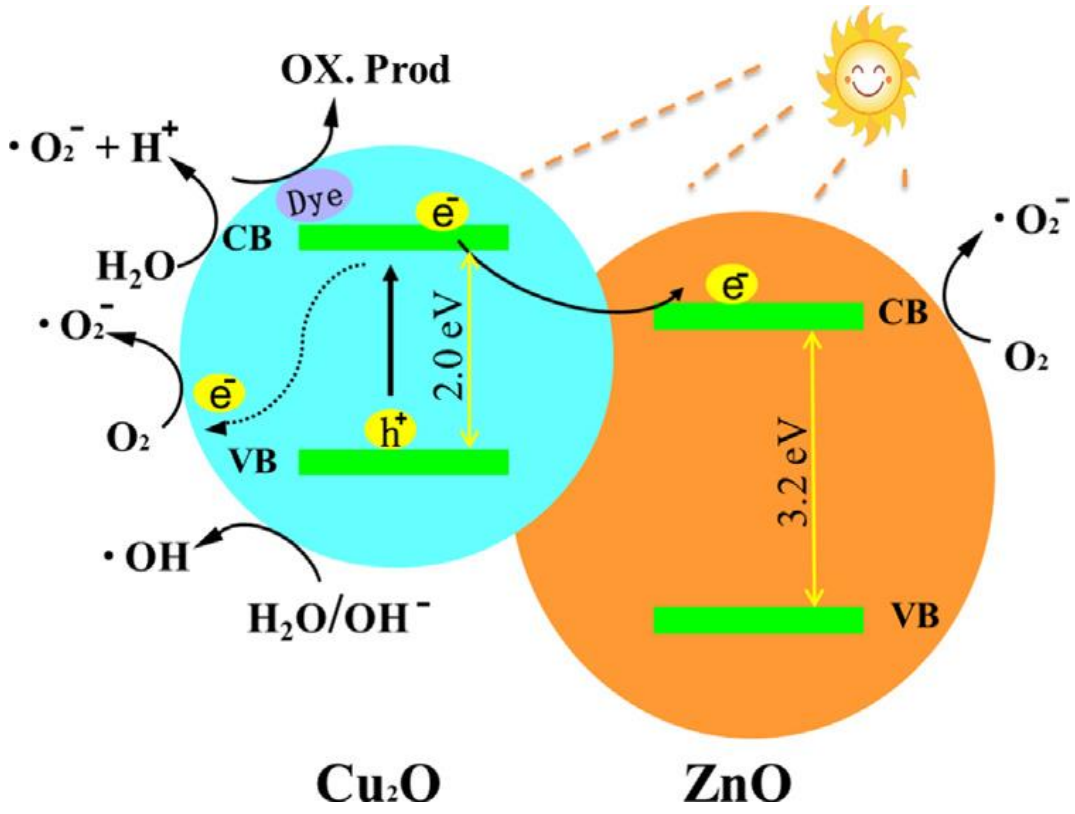

Figure1.The electrons in the CB of Cu_2O generated by visual light can transfer to the CB of ZnO.

The nanocomposite can form p–n semiconductor when p-type Cu_2O is loaded on n-type ZnO semiconductor's surface. The Fermi levels equalize in two semiconductors, and charge compensation occurs when the Cu_2O/ZnO is under thermal equilibrium. The conduction band position of ZnO is lower than that of Cu_2O (Jiang *et al*., 2013), so theoretically speaking, the generated electrons in Cu_2O can be transferred to ZnO.

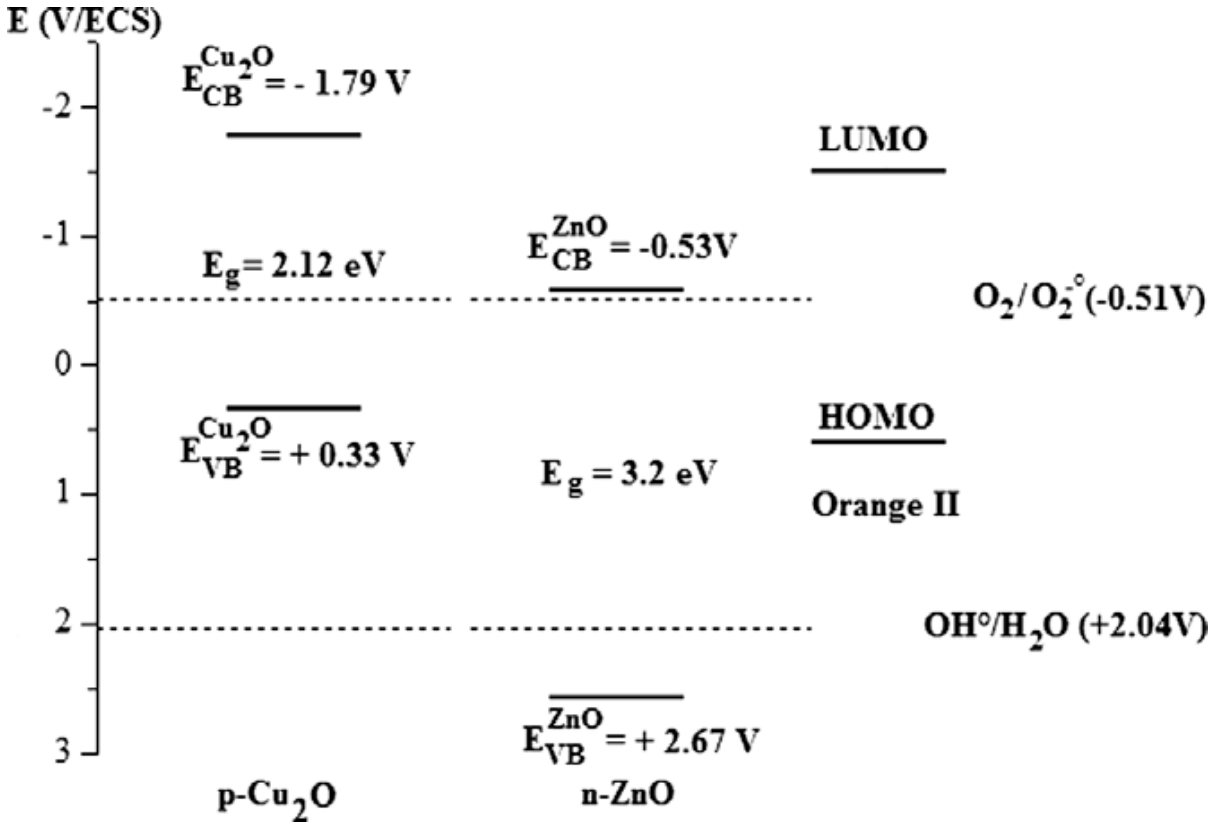

Figure.2. The electrons transfer from Cu_2O to ZnO.

The electrons transfer from ZnO to Ag_3PO_4 not only suppresses the recombination of photogenerated electrons and holes but also facilitates the OH radicals generation in the valence band (VB) of ZnO, and thus has significant influence on the visible light photocatalytic degradation of the organic dye. This is B-type heterojunction. And both the CB and VB of ZnO are higher than that of Ag_3PO_4 .Under visible light irradiation, the electrons in the VB of ZnO can be transferred to that of Ag_3PO_4. As a result, the holes generated in the VB of ZnO can induce photocatalytic oxidation reactions, while the produced electrons remain in the CB of Ag_3PO_4 particle can be used for photocatalytic reduction reactions. As the CB decreases in energy in the order of Ag_3PO_4< ZnO forming a stepwise band gap structure, the photogenerated electrons would most likely accumulate in the CB of Ag_3PO_4 (Chan *et al*., 2013). In this reaction mechanism, the photogenerated electrons in the Ag_3PO_4 CB would then participate in the reduction of dissolved oxygen (O_2) into superoxide ($HOO^{\bullet}$) or hydroxyl radicals ($^{\bullet}OH$); meanwhile the photogenerated holes likely oxidize H_2O to form $^{\bullet}OH$.

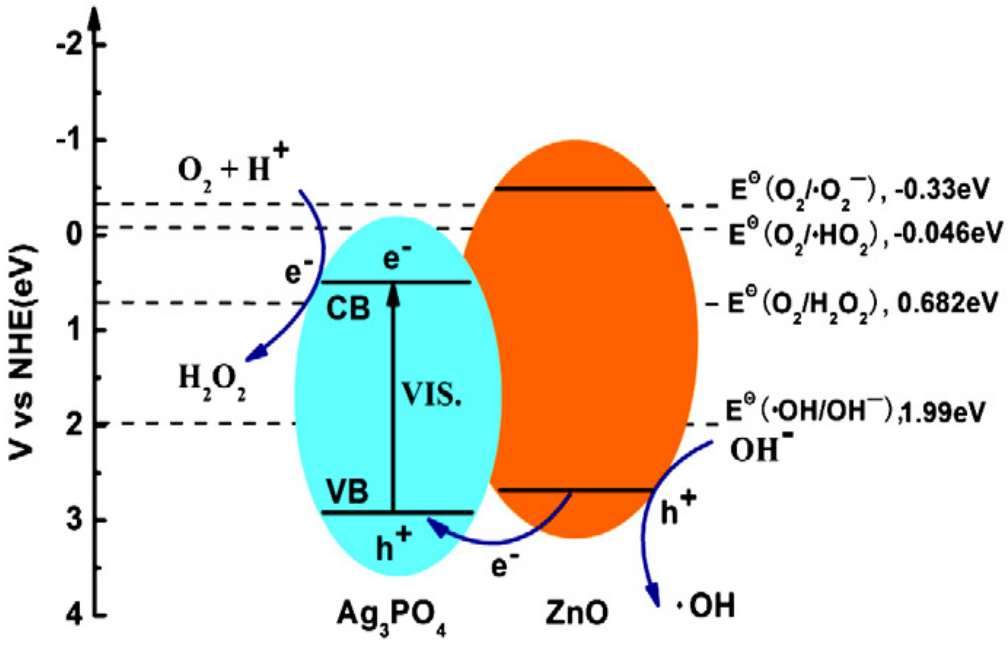

Figure.3. The formation of Ag_3PO_4/ZnO composite heterostructure

Generally the CB decreases in energy in the order of Ag_3PO_4< ZnO < Cu_2O forming a stepwise band gap structure, the photogenerated electrons would most likely accumulate in the CB of Ag_3PO_4 (Chan *et al*., 2013); meanwhile the photogenerated holes moved to the VB of Cu_2O, leading to effective charge separation.

2.1.2. Photocatalytic Degradation

Photocatalysis is a process by which a semiconductor material absorbs photon of energy equal to or greater than its band gap energy, there by generating electrons and holes at conduction and valence band, respectively, which can further generate free hydroxyl radicals in the system. The resulting free radicals are very efficient oxidizers of organic molecules (Pouretedal *et al*., 2009).The positive hole oxidizes either pollutant molecules directly or water to produce OH radicals, whereas the electron in the conduction band reduces free oxygen adsorbed on the surface of the photocatalyst (Ahmed *et al*., 2010).

Oxidation Reaction:

$$h^+ + \text{dye} \rightarrow \text{Dye}^*$$

$$h^+ + H_2O \rightarrow HO^{\cdot} + H^+$$

Reduction reaction:

$$\text{Dye} + {}^{\cdot}OH \rightarrow CO_2 + H_2O + \text{nontoxic minerals}$$

The ZnO/Ag/CdO nanocomposite removes the colour of textile effluent, but still the complete removal of toxic components and mineralization needs to be further confirmed.

$$\%\text{Degradation} = (Ao - At/\ Ao\ ) \times 100$$

where Ao is absorbance of dye at initial stage, At is absorbance of dye at time "t".

2.1.3. Determining the Rate Law from Experimental Data

Kinetics is the study of time-dependent processes two important reasons for investigating the rates of chemical processes. To determine how rapidly reactions attain equilibrium, and to understand information on reaction mechanism. There are three basic ways to determine rate laws and rate constants : using initial rates, directly using integrated equations and graphing the data, and using nonlinear least-squares analysis.

A kinetics experiment consists of measuring the concentrations of one or more reactants or products at a number of different times during the reaction. Make a series of measurements of the initial rate of the reaction with different initial concentrations [A]0. Measured concentrations as a function of time, may compare their time dependence with the appropriate integrated rate laws. The most commonly encountered ones are: Zeroth order integrated rate law: [A] = [A]0 – kt A plot of [A] vs t will be linear, with a slope of -k. First order integrated rate law: ln[A] = ln[A]0 – kt A plot of ln[A] vs t will be linear with a slope of -k. Second order integrated rate law:1/[A] =1/[A]0 + 2kt A plot of1/[A] vs t will be linear with a slope of 2k. If none of these plots result in a straight line, then more complicated integrated rate laws must be tried. Half lives; Another way of determining the reaction order is to investigate the behaviour of the half life as the reaction proceeds.

2.1.4. Zeolite as a Supporte for Nanomaterial

Zeolites are naturally occurring aluminosilicate minerals with highly uniform sub-nanometre and nanometre scale crystalline structures. Zeolite crystals consist of a three-dimensional cross-linked $(Si/Al)O_4$ tetrahedral framework, in which each Al or Si atom occupies the vertex

of a network connecting four oxygen atoms. The framework structure contains cavities that allow for the movement and containment of ions and water molecules (Liu *et al*., 2008).

In general, there are two types of zeolites such as natural and synthetic zeolites. Natural zeolites are cheaper and more abundant, but have smaller channels as compared with synthetic zeolites. As a natural mineral resource, natural zeolites are easy to obtain and cause negligible chemical pollutions during the production process (Anandan *et al*., 2003). Synthetic zeolites are also three-dimensional, microporous, crystalline solids with well-defined structure made by crystallization of sodium alumina-silicate gels prepared from pure sodium aluminate, sodium silicate and sodium hydroxide solutions. Zeolites have a variety of industrial applications, especially as ion exchangers, adsorbents, and chemicals catalysts.

Zeolites are a group of microporous, aluminosilicate minerals that have excellent adsorbing properties. They contain a number of alkali and alkaline-earth ions such as Na, K, Ca, Mg and Al. Some of the types of such zeolites includes natrolite, stilbite, phillipsite etc. They are generally formed in those places wherein volcanic ash can get in contact with water and reacts with it. Since zeolites largely consists a large number of pores of different pore diameters, it is capable of selectively photocatalytic reactor and then coating the catalyst as a uniform layer over the reactor walls. Natural clay minerals are promising support materials because they exhibit high specific surfaces areas, large pore volumes, chemical stability and good mechanical properties and they are commercially available in large quantities (Dong *et al*., 2012).

2.2. Factors Affecting Photocatalytic Degradation of Dye

2.2.1. Dye Type and pH Effect

Dyes are extensively used in textile, leather, newsprint recycling and the dye-house wastewater usually comprises various dyes, which are toxic and harmful for both human and aquatic lives. Hence, before discharging into the environment, treatment of dye waste water is an important issue (Malik, 2003).

The adsorbent concentration is an important parameter because this determines the capacity of the adsorbent for a given initial dye concentration. An increase in the adsorption rate with

adsorbent dosage can be attributed to increase surface area and the availability of more adsorption sites (Rajoriya *et al.*, 2011).

The overall degradation of MB proceeds through the following reaction,

$$C_{16}H_{18}N_3SCl + 25.5O_2 + hv + Ti02 \rightarrow HCl + H_2SO_4 + 3HNO_3 + 16CO_2 + 6H_2O$$

where, anodic and cathodic reactions can be expressed as follows

Anodic (oxidation) reaction:

$$h^+ + H_2O \rightarrow H^+ + OH^\cdot$$

Cathodic (reduction) reaction

$$e^- + O_2 \rightarrow O_2^- \rightarrow H_2O_2 \rightarrow H_2O \rightarrow \text{Degradation of MB}$$

Figure.4. Structure of methylene blue

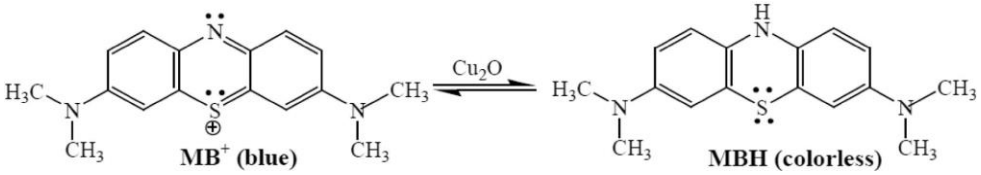

Figure.5. Decolorization of methylene blue dye in presence of Cu_2O NPs.

Power of hydrogen is recognized as one of the important parameters that governs the adsorption process. The solution pH would affect both aqueous chemistry and surface binding sites of the adsorbent. So the solution pH is an important parameter during the dye adsorption process. It is known that the solution pH can affect the surface charge of the adsorbent, the degree of ionization of the different pollutants, the dissociation of functional groups on the active sites of the adsorbent as well as the structure of the dye molecule (Zhang *et al.*, 2011).

2.2.2. Effect of Photocatalyst Load Under Visible Light

An optimum photocatalyst concentration is important for avoiding excess photocatalyst and ensuring total adsorption of efficient photons. When the amount of TiO_2 increases above a saturation level (leading to a high turbidity state), the light photon absorption coefficient usually decreases radially. However, such a light attenuation over the radial distance could not be well correlated with the BeereLambert Law owing to the strong absorption and scattering of light photons by the TiO_2 particles (Chen *et al*., 2007). The excess TiO_2 particles can create a light screening effect that reduces the surface area of TiO_2 being exposed to light illumination and the photocatalytic efficiency. Therefore, any chosen photoreactor should be operated below the saturation level of TiO_2 photocatalyst used to avoid excess catalyst and ensure efficient photons absorption. In this sense, both catalyst loading and light scattering effect can be considered as a function of optical path length in the reactor. A large number of studies have reported the effect of TiO_2 loadings on the process efficiency (Gaya and Abdullah, 2008; Herrmann, 1999). These results are mostly independent and a direct comparison cannot be made, as the working geometry, radiation fluxes, intensity and wavelengths used were different. It was reported that the optimum catalyst loading for photomineralization and photo-disinfection are varied, and mainly depend on the dimension of the photoreactor. In addition, the determination of photoreactor diameter is crucial in not only the effective photons absorption but also the water flow hydrodynamics (Malato *et al.*, 2009). Uniform flow region can ensure that a steady state residence time is obtained, while turbulence flow removes catalyst deposition or reaction dead zone.

Concentration of TiO_2 in the photocatalytic water treatment system affects the overall photocatalysis reaction rate in a true heterogeneous catalytic regime, where the amount of TiO_2 is directly proportional to the overall photocatalytic reaction rate (Gaya and Abdullah, 2008). A linear dependency holds until certain extent when the reaction rate starts to aggravate and becomes independent of TiO_2 concentration. This is attributed to the geometry and working conditions of the photoreactor where the surface reaction is initiated upon light photon absorption (Bamba *et al.*, 2008).

In any given photocatalytic application, the optimum catalyst concentration must be determined, in order to avoid excess catalyst and ensure total absorption of efficient photons.

This is because an unfavourable light scattering and reduction of light penetration into the solution is observed with excess photocatalyst loading. Further increase in load, however, resulted in decreased photodecomposition efficiency because of suppressed active sites due to particle aggregation.

2.2.3. Effect of Initial Concentration of Dye

The effect of initial dye concentration on the photocatalytic degradation efficiency of the catalyst tends to decrease at higher concentration. This leads to think that there should be a maximum dye coverage allowing efficient reaction at the active sites. Since, the possibility of photocatalyst excitation diminished at higher concentration levels, the screening effect also dominates and hence, degradation efficiency decreased (Nezamzadeh-Ejhieh *et al.*, 2012).

2.2.4. Effect of Temperature

Numerous studies have been conducted on the dependence of photocatalytic reaction on the reaction temperature. Although heat energy is inadequate to activate the TiO2 surface, the understanding on such dependency could be extrapolated when operating the process under natural sunlight illumination. Most of the previous investigations stated that an increase in photocatalytic reaction temperature (>80 C) promotes the recombination of charge carriers and disfavour the adsorption of organic compounds onto the TiO_2 surface (Gaya and Abdullah, 2008). A further reaction in temperature down to ^{0} C will cause an increase in the apparent activation energy. As a consequence, the optimum reaction temperature for photomineralization is reported to be in the range of 20-80 ^{0} C (Malato *et al*., 2009).

2.3. Degradation Mechanism of Methylene Blue

According to the degradation pathway of methylene blue, OH radical makes the main contribution to degradation of methylene blue and its intermediates. Since the MB is cationic and not electron donor, the initial step of MB degradation can be ascribed to the cleavage of the bonds of C–S^+=C functional group in MB:

$$R–S^+=R' + OH^\cdot \rightarrow R–S(=O)–R' + H^+ \qquad (1)$$

The sulfoxide group can undergo a second attack by an OH· radical producing the sulfone and causing the definitive dissociation of two benzenic rings:

$NH_2{-}C_6H_3(R){-}S(=O){-}C_6H_4{-}R + OH^{\cdot} \rightarrow NH_2{-}C_6H_3(R){-}SO_2 + C_6H_5{-}R,$ (2)

and/or

$NH_2{-}C_6H_3(R){-}S(=O){-}C_6H_4{-}R + OH^{\cdot} \rightarrow NH_2{-}C_6H_4{-}R + SO_2{-}C_6H_4{-}R$ (3)

Subsequently, the sulfone can be attacked itself by a third OH· radical for giving a sulfonic acid:

$SO_2{-}C_6H_4{-}R + OH^{\cdot} \rightarrow R{-}C_6H_4{-}SO_3H$ (4)

Finally release of SO_4^{2-} ions can be attributed to a fourth attack by $OH^{\cdot}$:

$R{-}C_6H_4{-}SO_3H + OH^{\cdot} \rightarrow R{-}C_6H_4^{\cdot} + SO_4^{2-} + 2H^{+}$ (5)

The amino group in MB can be substituted by an OH· radical, forming the corresponding phenol and releasing a $NH_2^{\cdot}$ radical which generates ammonia and ammonium ions, estimated to be primary products.

$R{-}C_6H_4{-}NH_2 + OH^{-} \rightarrow R{-}C_6H_4{-}OH + NH_2^{\cdot},$ (6)

$NH_2^{\cdot} + H^{\cdot} \rightarrow NH_3,$ (7)

$NH_3 + H^{+} \rightarrow NH_4^{+}.$ (8)

The other two symmetrical dimethyl-phenyl-amino groups in MB undergo a progressive degrading oxidation of one methyl group by an attack from $OH^{\cdot}$ radical, producing an alcohol, then an aldehyde, which is spontaneously oxidized into acid, decarboxylates into CO_2 by photo-Kolbe reaction. Although some degradation pathways of degrading MB have been presented based on detected reaction intermediates, a thorough degradation mechanism is still difficultly put forward since many intermediates have certainly formed, but are difficult to detect.

2.4. Method to Synthesis Nanomaterials

There are various methods available for synthesis of metal oxide nanoparticle comprising mainly of liquid phase, gas phase, liquid-based gas phase, co-precipitation, microemulsion/ direct/inverse micelle approach, sol–gel, hydrothermal and template/ surface derived methods. Due to their unique and improved properties in relation to size, composition and structure, metal oxide nanoparticles are of considerable interest for a wide variety of applications as discussed (Koziej *et al*., 2014). The method employed for immobilising the photocatalyst material on the support, plays a significant role in determining the photocatalytic activity of the photocatalyst. Hence, a good choice of supporting medium is often required, depending on the type of catalyst used and the pollutant molecule to be degraded. The technique followed for the deposition must be such that, it does not reduce the photo catalytic activity of the photocatalyst. Many methods have been reported in the literature to accomplish the same. Some of these methods includes sol gel method, primarily consisting of dip coating (Sonawane *et al.,* 2003; Vaiano *et al*., 2015), chemical vapour deposition (CVD) which includes techniques such as, atmospheric pressure chemical vapour deposition (APCVD), plasma enhanced chemical vapour deposition (PECVD), metaleorganic chemical vapour deposition (MOCVD) and hybrid physical chemical vapour deposition (HPCVD), thermal treatment method, electrophoretic deposition and (Cao *et al*., 2014; Zuo, 2010). Most of these techniques however are not used widely as they require high temperature calcination which can cause decomposition of the substrate, complex procedures and expensive instrumentation.

2.4.1. Co- Precipitation Method

Precipitation is similar to crystallization except that the driving force in the latter is solubility, whereas in the former it is a chemical reaction. When the product of any of these solution phase chemical reactions is an insoluble product, it is called a precipitation reaction. Because of the ability to control kinetics with variations in temperature and solvent type, precipitation reactions are among the most versatile synthetic methods. Lanje *et al. (*2013) used the cost competitive and simple precipitation process for the synthesis of zinc oxide. The single step process with the large scale production without unwanted impurities is desirable for the cost-effective preparation of ZnO nanparticles. A facile and convenient method to prepare nanoparticles is chemical co-precipitation technique. Two or more soluble salts solutions are

mixed in a definite ratio and co-precipitated with a base solution under inert atmosphere. Co-precipitation involves taking a stoichiometric mixture of soluble salts of the metal and precipitating them as hydroxides, citrates, oxalates, or formates. The mixture is filtered, dried, and then heated to give the final product.

2.4.2. Top Down and Bottom up Synthesis

Top down approach refers to successive cutting of a bulk material to get nano sized particles. Bottom up approach refers to the buildup of a material from atoms or molecules. Both the top-down and bottom-up approaches may be carried out in gas, liquid or solid states, with a variety of different applications. These applications have their interest in controlling particle size, particle shape, size distribution, particle composition and degree of particle agglomeration. The biggest problem with the top-down approach is that it introduces internal stress, surface defects and contaminations (Jyoti *et al*., 2008).

2.4.3. Sol–gel Processing

The sol–gel process is currently considered one of the most promising alternatives due to its inherent advantages including low sintering temperature, versatility of processing and homogeneity at molecular level. The This phase has been extensively investigated because of its high activity in photocatalytic applications . One of the advantages of sol-gel synthesis of mesoporous materials is the possibility to form uniform films on a substrate. Sol–gels have been used as templates for directing micro and nano-scale materials morphology, which will be explained further shortly. Nanoparticles for membrane applications are most often prepared through the sol–gel process, which yields high purity samples and allows for control over size, composition, and surface chemistry. The sol-gel polymerization of metal alkoxides in presence of inorganic salts lead to the formation of ceramic oxides materials with important micro structural properties.

The sol-gel process is a simple technique that is primarily use in the fabrication of metal oxides using the corresponding metal ion containing chemical solutions as starting materials. These precursors play a crucial role on deciding the morphology of thedeposited photocatalyst particles. These precursors may produce an extensively integrated (gel-like) network of discrete particles or polymers. The sol-gel approach is a low-cost, low-temperature technique

that can accurately control the chemical composition of the end product. Even small quantities of dopants, such as organic dyes (in case if dye sensitized photocatalyst is required) or rare earth elements, can be introduced in the coating sol and will eventually end up uniformly dispersed in the final product. Generally, metal alkoxides and metal chlorides are the precursors used in the process. These compounds undergo a variety of hydrolysis and condensation reactions to produce inter-linked connections of metal centres (M) that are connected by oxo (MO-M) or hydroxy (M-OH-M) linkages. Any excess solvent present is often removed by drying process, which ultimately causes volume shrinkage and densification of the photocatalyst film. The drying is followed by a thermal treatment process, which favors further poly-condensation and enhances the mechanical properties and structural stability of the films by sintering, densification, and grain growth.

The inherent advantages of this method include: lower temperature of preparation, better purity of deposits from a given raw material, better homogeneity from a given raw material, effective control over the particle size, shape, distribution and properties, the possibility of tuning the material structure by changing the solvent used or by using other supports for coating, provides better mixing for multicomponent mixtures, new non-crystalline solids can be produced even outside the range of normal glass formation. (Exposito *et al.*, 2017) immobilised the TiO_2 onto glass plates in a rotating disc reactor (RDR) by using the solegel method reported elsewhere by (Boiarkina *et al*., 2013) to study the degradation of antipyrene.

Draw backs of sol-gel method: cost of precursors; shrink age of a wet gel up on drying, which often leads to fracture due to the generation of large capillary stresses and, consequently, makes difficult the attainment of large monolithic pieces; preferential precipitation of a particular oxide during sol formation (in multicomponent glasses) due to the different reactivity of the alkoxide precursors; difficult to avoid residual porosity and OH groups.

2.4.4. Hydrothermal Method

The hydrothermal method involves heating the reactants in a closed vessel (an autoclave). An autoclave is constructed from thick stainless steel and fitted with safety valves. One of the most common techniques of immobilisation in present day research is PAHD or polymer assisted hydrothermal decomposition which is technical combination of polymer assisted

deposition and hydrothermal methods. In addition, PAHD plays a vital role in water soluble polymers, they have the ability to control viscosity as well as bond with the metal ions thereby reducing hydrolysis. Thus, PAHD avoids irregular morphology and broad distribution of particle size. Another advantage of this method is that it usually forms films with thicknesses as large as tens of microns, much thicker than films. PAHD is a simpler and inexpensive process, when compared to other immobilization techniques that enables the formation of a range of high quality materials by means of an accurate control of the stoichiometric ratio of precursor solutions, polymers, and dopants, for multi-phase materials.

2.5. Characterization of Photocatalyst Nanoparticles

2.5. 1. X-ray Diffraction Method

In order to determine the crystal phase composition and the crystallite size of the photocatalyst, a powder X-ray diffraction method (XRD) study should be carried out. The XRD pattern of the nano-sized Ag_3PO_4 products exhibited well-defined peaks indicative of highly crystalline Ag_3PO_4 with body-centered cubic structure. The diffraction pattern and spacing closely matched to the diffraction pattern of the bulk ZnO. It is known that the photocatalytic activity is mainly governed by phase structure, adsorption ability, and separation efficiency of photogenerated electrons and holes.

$$D = \frac{K\lambda}{\beta COS\theta}$$

Here, D is the crystal size of the catalyst, λ is the X-ray wavelength (1.54 Å), β is the full width at half maximum (FWHM), K k is scherrer constant (0.89) and θ is the diffraction angel.

The crystalline size of as-synthesized photocatalysts is one of the important physical factor under photocatalytic degradation process (Hosseinnie *et al*.,2010).The peaks allotted to diffractions from various planes correspond to hexagonal close packed structure of ZnO.

2.5.2. UV-Visible Absorption Method

Many semiconductors have been tested that utilize UV–vis irradiation to degrade a high number of recalcitrant materials in aqueous system. As TiO_2 photocatalytic reactions take place under ambient operating conditions, photoactivity is usually constrained by the narrow wavelength spectrum for photonic activation of catalysts. The point where the blue shift occurs favoring surface recombination of electron–hole pairs and allowing for the maximum number of active sites per mass of catalyst (Zhang, *et al*., 2011). The higher-end of UV spectrum required for catalysts activation is usually accompanied by high operating costs. One attractive option is to utilize the vast abundance of outdoor solar irradiation for catalyst activation in a suitably designed photoreactor system. For UV irradiation, its corresponding electromagnetic spectrum can be classified as UV-A, UV-B and UV-C, according to its emitting wavelength. The UV-A range has its light wavelength spans from 315 to 400 nm (3.10-3.94 eV), while UV-B has wavelength range of 280 to 315 nm (3.94-4.43 eV) and the germicidal UV-C ranges from 100 to 280 nm (4.43-12.4 eV) (Rinco´n and Pulgarin, 2005). UV–vis diffuse reflectance spectroscopy is carried out to investigate the optical properties of the as-synthesized nanophotocatalyst samples. The UV–vis diffuse reflectance spectra of Ag_3PO_4 nanoparticles shift to longer wavelength (max. at 475 nm) indicating they are highly visible light active semiconductors.

2.5.3. TEM/SEM Microscope

Transmission electron microscopy (TEM) is one of the more popular tools to study nanoparticles. It is capable of a resolution at 0.1 nm (high resolution TEM), and provides 2 Dimension information about nanoparticles dispersion, structure, and shape. Scanning electron microscopy (SEM) has a lower resolution than TEM, but provides surface information. For a chemical analysis, optional tools incorporated in TEM/SEM microscopes, such as the energy dispersive X-ray analysis, provide localization of elements in a semi quantitative manner.

2.5.4. Fourier-Transformed Infrared Spectroscopy (FT-IR) Method

.Infrared spectroscopy is a technique for determining the functional groups within the compounds. The FT-IR spectrum range of the usage is in the mid infrared region which covers the frequency from 400-4,000 cm^{-1}. Persenaire *et al* (2001) proposed a degradation mechanism

based on the results obtained from high resolution thermo gravimetric analysis coupled to mass spectrometry (MS) and Fourier transform infrared spectrometry.

3. MATERIALS AND METHODS

3.1. Experimental Site

Synthesis of Cu_2O-Ag_3PO_4-ZnO nanomposite and zeoliet supported Cu-Ag-Zn mixed nanocomposites, photocatalytic degradation, UV-Visible study were conducted at Haramaya University research laboratory. XRD Characterization were conducted in Adama University.

3.2. Apparatus and Equipments

During synthesis and characterization of the as-synthesized photocatalyst nanoparticles, the following materials and equipments was used: Uv-visible spectrophotometer (SANYO sp65), X-ray diffraction, reactor tube, oven, analytical balance, deionizer, furnace, ceramic crucibles, centrifuge, volumetric flasks, bottle, pipettes, graduated cylinders, magnetic stirrer with hot plate, test tubes, funnels, filter papers, Mortar and pestle, thermometer and beakers.

3.2.1. Reagents and Chemicals

For the synthesis of Cu_2O-Ag_3PO_4-ZnO nanoparticles the following chemicals were used: copper (II) chioride dehydrate ($CuCl_2 \cdot 2H_2O$), Ascorbic acid ($C_6H_8O_6$), silver nitrate ($AgNO_3$), disodium hydrogen phosphate (Na_2HPO_4), Sodium hydroxide (NaOH, MW 40 g/mol, 99.0%, FLUKA (Switzerland), hydrochloric acid (HCl, MW: 36.5 g/mol, Min Assay 99.0%) and double distilled water agar, zinc nitrate hex hydrate Zn $(NO_3)_2.6H_2O$, sodium carbonate(Na_2CO_3), Natural zeolite , Methylene blue(MB).

3.3. Methods and Procedures

3.3.1. Synthesis of Cu_2O-Ag_3PO_4-ZnO Ternary Composite

The ternary nanocomposite was synthesized according to the procedure developed by (Dong *et al*., 2006). Nanocomposite of Cu_2O-Ag_3PO_4-ZnO were prepared by precipitation method. In 0.1 M solutions, 3.45 g of copper (II) chloride dehydrate ($CuCl_2 \cdot 2H_2O$), 1.41 g of Ascorbic acid ($C_6H_8O_6$), 2.12 g of sodium carbonate (Na_2CO_3), 1.7 g of silver nitrate ($AgNO_3$), 1.42 g of disodium hydrogen phosphate (Na_2HPO_4), 20.82 g of zinc nitrate hexahydrate (Zn $(NO_3)_2.6H_2O$) and 7.42 g of sodium carbonate (Na_2CO_3) were dissolved in 500 ml of

deionized water separately using magnetic stirring for 1 hr. Consequently, these solutions in the separate beakers were mixed together under magnetic stirring for 2 hr and filtered using filter paper. The product was washed three times with double deionized water and dried in an oven at 80^{o}C for 9 hr to form the precursors of Cu_2O-Ag_3PO_4-ZnO. Finally, the precursors were calcined at 300^{o}C for 2 hr in Nitrogen Bergen Furnace. The final sample were ground into powder and then used for the study of photocatalyst.

3.3.2. Preparation of Zeolite Supported Cu_2O-Ag_3PO_4-ZnO Nanocomposite.

The zeolite supported material was prepared by solid state reaction of the Cu_2O-Ag_3PO_4-ZnO photocatalyst and natural zeolite in two ratios (35:65 and 50:50) respectively. In both cases, the slurry was stirred for 1 hr at 80^{o}C for each case. After solvent evaporation, the solids were dried and crushed by grinding in mortar and pestle for the formation of homogenous solid state mixture. The powdered mixtures were then calcined in air at 300^{o}C for 1 h to get the zeolite supported nanocomposites (Tedla *et al*., 2015).

3.4. Characterization of Photocatalysts

3.4.1. XRD Method

The X-ray diffraction patterns of as synthesized photocatalysts were obtained using a BRUKER D8 (West Germany) X-ray diffractometer (XRD) equipped in Adama University The average crystalline sizes of as-synthesized nanoparticles was calculated by using Debye Scherrer formula:

$$D = \frac{K\lambda}{FWHM\cos\theta}$$

Where D is crystallite size in nm, K is the shape factor constant which is equal to 0.94, λ is the x-ray wave length, and FWHM is the full width at half maximum (in radians) for a diffraction occurring at 2θ (in degrees).

3.4.2. Uv/vis Spectrophotometer Method

The absorbance of the clear solution was measured at maximum absorption wave length using Uv/vis spectrophotometer for quantitative analysis. Photocatalytic degradation of nanocomposite were monitored spectrophotometrically.

$$\%\, Degradation = \frac{A_{O-A}}{A_O} \times 100$$

A_o is dye initial absorbance before irradiation and A is the absorbance of dye at irradiation time. Photocatalytic degradation activities of the nanocomposites under visible light irradiation have been evaluated for a model pollutant methylene blue (MB) dye solution.

3.5. Kinetic Study of Photocatalytic Degradation

The Kinetics of the photocatalysis rates of MB dye concentrations were calculated by relating kinetic parameters for dye at different concentrations. The pseudo-first- and pseudo-second order models was applied in order to find an efficient model.

4. RESULT AND DISCUSION

4.1. Characterization of the As-Synthesized Nanocomposite

4.1.1. XRD Analysis

X-ray diffraction patterns of the synthesized unsupported and subsequently supported Cu_2O-Ag_3PO_4-ZnO (20:10:70 ratios) nanostructured composites are illustrated in figure 6. The diffraction peaks observed at scattering angles 2θ values for the unsupported NCS of Cu_2O-Ag_3PO_4-ZnO (20:10:70 ratios) is depicted in figure 6. The diffraction peaks at 2θ values of 42.21, 61.3 and 73.56 can possibly represent cubic structure of Cu_2O nanoparticles. Diffraction peaks at 2θ values of 29.57 and 36.39 could be ascribed to the body centered cubic structure of Ag_3PO_4 nanoparticles. Whereas the remaining peaks observed at 2θ values of 31.61, 34.15, 36.27, 38.11, 44.8, 64.45 and 77.42 could be attributed to the formation of pure hexagonal wurtzite structure of ZnO (Srideve and Rajendran, 2009). The sharp and intense peaks from figure 6 below confirm the good crystalline nature of ZnO nanoparticles. The above finding evidences the presence of the desired components the ZnO crystal being the host in the ternary unsupported nanocomposite system.

The diffraction peaks of supported NCS consists of unsupported 50% NCS Cu_2O-Ag_3PO_4-ZnO (20:10:70) ratios and 50% of natural zeolite mixture from figure 6 below confirm that the diffraction peaks at 2θ values ranging from 11.26 to 27.8 could be associated to the zeolite supported nanocomposite (Tedla et al., 2015). Apart from this, peaks associates with each metal component are also observed, the peaks at 2θ values of 32.03 and 61.7 are responsible for Cu_2O whereas the peaks at 2θ values of 30.1 and 56.63 in the supported system could be ascribed to Ag_3PO_4 nanoparticles. The diffraction peaks at 2θ values of 22.43, 35.54 and 38.10 being attributed to the major peaks of ZnO nanoparticle for supported nanocomposite.

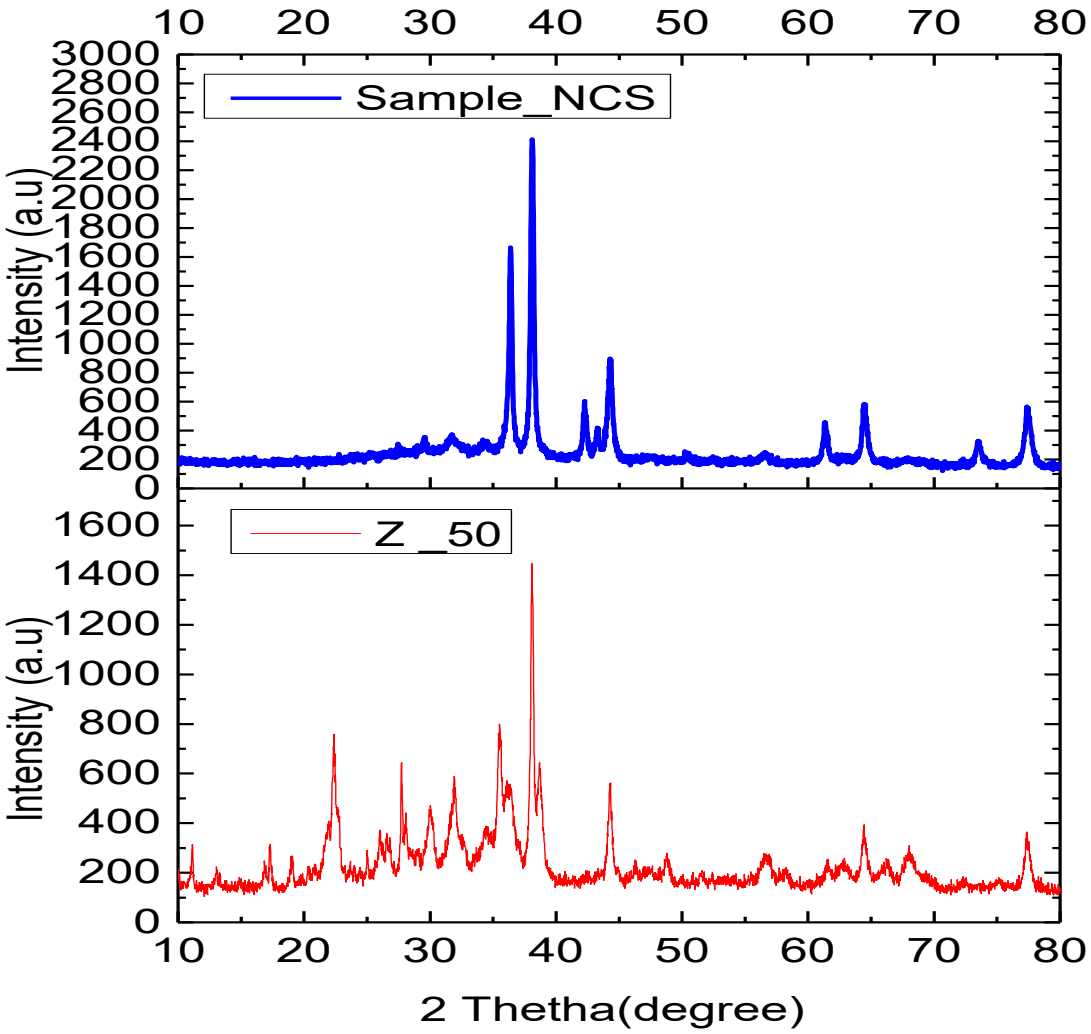

Figure. 6: XRD Plot for Sample_NCS and Z_50 NCS.

The average crystallite sizes of the as-synthesized unsupported and supported nanocomposite were obtained using Debye-Scherrer formula

$$D=K\lambda/\beta\cos\theta$$

Where, *D* = crystallite size in nm, *K* = the shape factor constant and taken as 0.9; β is the full width at half maximum (FWHM) in radians, λ is the wave length of the X-ray for Cu target Kα1 radiation and θ is the Bragg's angle.

The calculated average crystalline size of as-synthesized photocatalysts is recorded in Table 1.

Nanocomposite	2θ (degree)	β (radians)	D (nm)
Unsupported Ncs	38.11	0.0049	46.63
Supported Ncs (Z50Ncs)	38.10	0.0045	50.85

The result show that in table 1 above, the average crystalline sizes of unsupported and supported nanocmposite become 46.63nm and 50.85nm respectively recorded which is favorable for photocatalytic reaction. The rate of decolorization of organic dyes increases as the particle size decreases. This is because of increase in the specific surface area of a photocatalyst as the crystalline dimension decrease. Photocatalytic degradation activities of the nanocomposites under visible light irradiation have been evaluated for a model pollutant methylene blue (MB) dye solution. The crystalline size of as-synthesized photocatalysts is one of the important physical factor under photocatalytic degradation process (Hosseinnie *et al*.,2010).

4.2. Photocatalytic Studies Cu_2O-Ag_3PO_4-ZnO Ternary Composite

4.2.1. Comparison of Photocatalytic Activities of the As-synthesized Nanocomposite

The photocatalytic activities of all sample, Cu_2O-Ag_3PO_4-ZnO ternary nanocomposite (20:70:10), Zeolite 35% nanocomposite and Zeolite 50% Cu_2O-Ag_3PO_4-ZnO nanocomposite using initial MB concentrations of 10, 20, 30, 40, 50 mg/L and with 60, 80, 100, 120 and 140 mg/L photocatalyst load were evaluated under visible light. The degradation process was monitored by an UV–vis absorbance spectrometer (measuring the absorbance of MB at 664 nm). The degradation of the MB was calculated according to the initial and final absorbance of MB in the solutions. For comparison, the highest % degradation of the photocatalysts unsupported Ncs, Z-35 Ncs and Z-50 Ncs were 72.82, 84.5 and 88.2 as indicated in figure 7 and Appendix Table 5 at 10 ppm MB with 120 mg photocatalyst. The degradation performance of Z-35 Ncs and Z-50 Ncs systems generally showed better catalytic efficiency compared to the unsupported catalysts systems. The zeolite matrices are also contributing to the delay in the recombination reaction by a hopping mechanism of electron in the framework (Dubey *et al*., 2006).

The photocatalytic degradation activity of as-synthesized nanocomposite under visible light irradiation and the highest percentage degradation were recorded in zeolite supported nanocomposite. Because zeolite serves as to supported nanocomposite which increases its surface area. This improves the generation of reactive radicals and thereby contributes to enhancement of MB photodegradation. Therefore, the active sites exposed for photocatalytic reaction increases as the surface area increases.

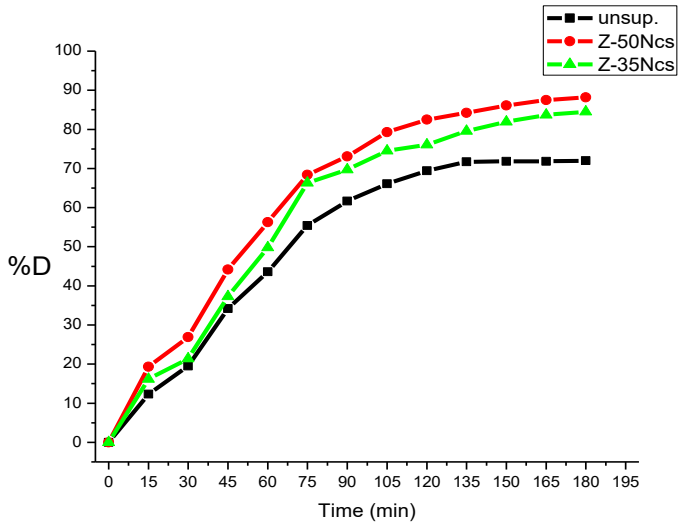

Figure.7. Plots of % degradation of MB as a function of time under visible irradiation using unsupported Ncs and supported photocatalysts: MB = 10 mg/L , catalyst load =120 mg/L.

4.2.2. Effect of Initial Dye Concentration

The effect of initial concentration on the degradation of MB was studied using different concentrations of the dye 10, 20, 30 and 40 mg/L by keeping the unsupported photocatalyst load 120 mg/L. According to figure 8 and appendix table 1, the highest recorded percentage degradation of MB at these concentrations was 72.82, 61.3, 49.4 and 35.2 respectively. From the above results, the highest degradation was found to be maximum at 10 mg/L initial concentration of MB as indicated in the figure 8. Photodegradation rate decreases when dye concentration increases. It is because at higher concentration of dye, the number of interacting radiation photons per dye molecule decreases.

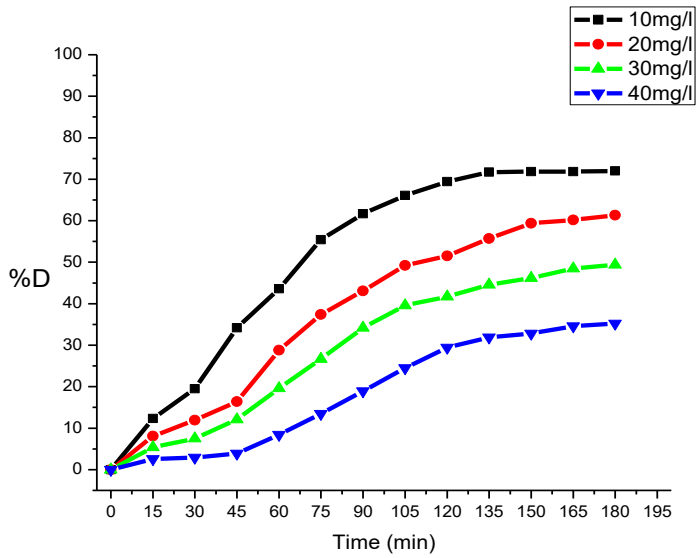

Figure.8. Plots of % degradation of MB as function of time under visible light irradiation by keeping the unsupported Ncs load constant(120mg/l) and varying the amount of MB solution.

The photocatalytic degradation efficiency of the supported composite is higher than unsupported photocatalyst under visible light irradiation for 180 min. The maximum degradation efficiency of 88.2% was Z50-Ncs under visible light. This due to the high surface area of zeolite (Tadle *et al*, 2013). The higher surface area of zeolite favors the adsorption of more water molecules, hydroxyl ions and dye molecules, thus leading to higher photoreactivity.

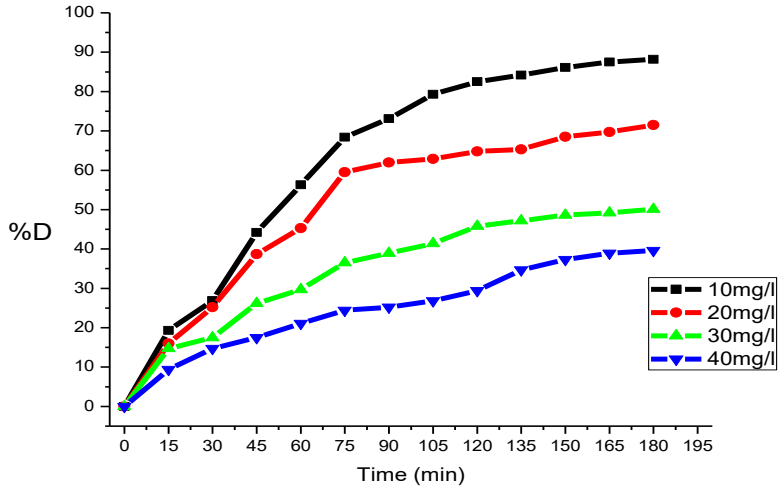

Figure.9. Plots of % degradation of MB as function of time under visible light irradiation by keeping the Z50-Ncs load constant(120mg/l) and varying the amount of MB solution.

4.2.3. Effect of Zeolite on Photocatalytic Degradation

The efficiency of the as-synthesized Cu_2O - Ag_3PO_4 –ZnO photocatalyst in different zeolite compositions for the degradation of MO solution under visible light irradiation, with an initial dye concentration of 10 mg/L, catalyst load of 120 mg/L was studied as a function of irradiation of time. Accordingly, the plot of percentage degradation as a function of irradiation time (Figure.9) indicates that the maximum percentage degradation 88.2% and 84.5% of MB dye occurred at the zeolite (50) Cu_2O- Ag_3PO_4 -ZnO and zeolite(35) Cu_2O-Ag_3PO_4-ZnO photocatalyst respectively. The zeolite matrices are also contributing to the delay in the recombination rxn by a hopping mechanism of electron in the framework. In addition to delaying electron hole recombination reaction, zeolite serves to supported Ncs which increases its surface area. Therefore, the active sites exposed for photocatalytic reaction increases as the surface area increases. The zeolite matrices are also contributing to the delay in the recombination reaction by a hopping mechanism of electron in the framework (Dubey *et al*., 2006).

4.2.4. Kinetic Study of Methylene Blue Degradation

Kinetic studies not only help us to determine the speed or rate of a chemical reaction but also describe the conditions by which the reaction rates can be altered. The factors such as concentration, temperature, pressure and catalyst affect the rate of a reaction. Kinetics of MB degradation determined the reaction kinetics for the degradation of aqueous methylene blue solution using the UV–vis absorbance data. According to first order reaction kinetics ln(Co/Ct) = kt, values of ln(Co/Ct) as a function of irradiation time are given in Appendix Table 2&4 and corresponding plot are shown in Figure 12 and13. From the linear correlation of the plot suggested that, photocatalitic degradation of MB was pseudo first order kinetics. Rate constant using different MB concentration using unsupported photocatalysts are 7.0 X 10^3 min^{-1}, 5.3 X 10^3 min^{-1}, 3.7 X 10^3 min^{-1}, 2.4 X 10^3 min^{-1} and the correlation constant R^2 for the fitted line was calculated to be 0.979, 0.981, 0.973, and 0.954 for MB concentration of 10, 20, 30 and 40 mgL^{-1}, respectively and Rate constant using different MB concentration using supported photocatalysts are 5.0 X 10^2 min^{-1}, 1.9 X 10^2 min^{-1}, 1.1 X 10^2 min^{-1}, 9.2 X 10^3 min^{-1} and the correlation constant R^2 for the fitted line was calculated to be 0.984, 0.919, 0.720, and 0.625 for MB concentration of 10, 20, 30 and 40 mgL^{-1}, respectively. It is known that the photocatalytic activity is mainly governed by phase structure, adsorption ability, and separation efficiency of photogenerated electrons and holes (Wang *et al*., 2011). One is the property of silver nanoparticles of becoming an electron reservoir by changing their oxidation state and suppressing the photogenerated electron–hole recombination in the nanocomposite subsystem. The other is the adsorptive capacity of the zeolitic matrices, which permits closer contact between the organic molecules and the supported nanoparticles by a local concentration effect.

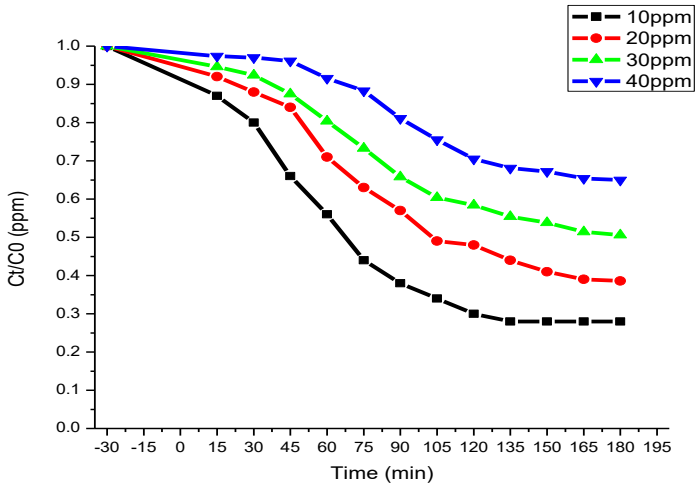

Figure.10. The corresponding comparison of different concentration of MB photodegradation under visible light irradiation Unsupported Ncs.

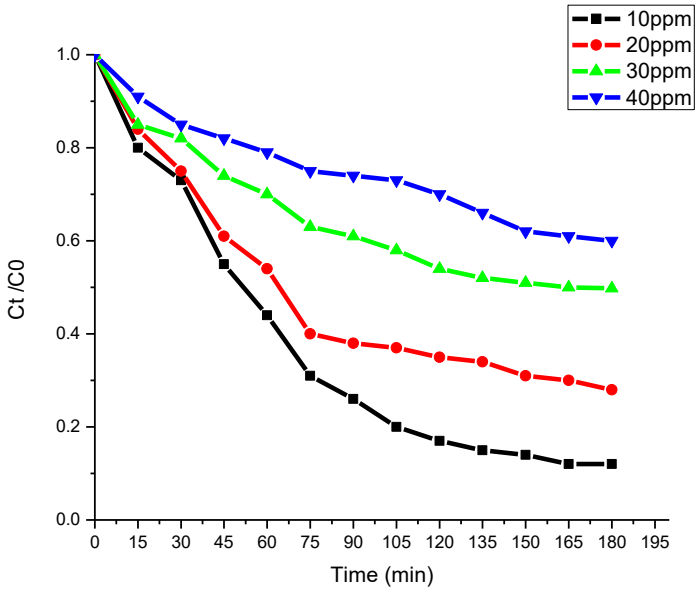

Figure.11.The corresponding comparison of different concentration of MB dye photodegradation under visible light irradiation supported Ncs.

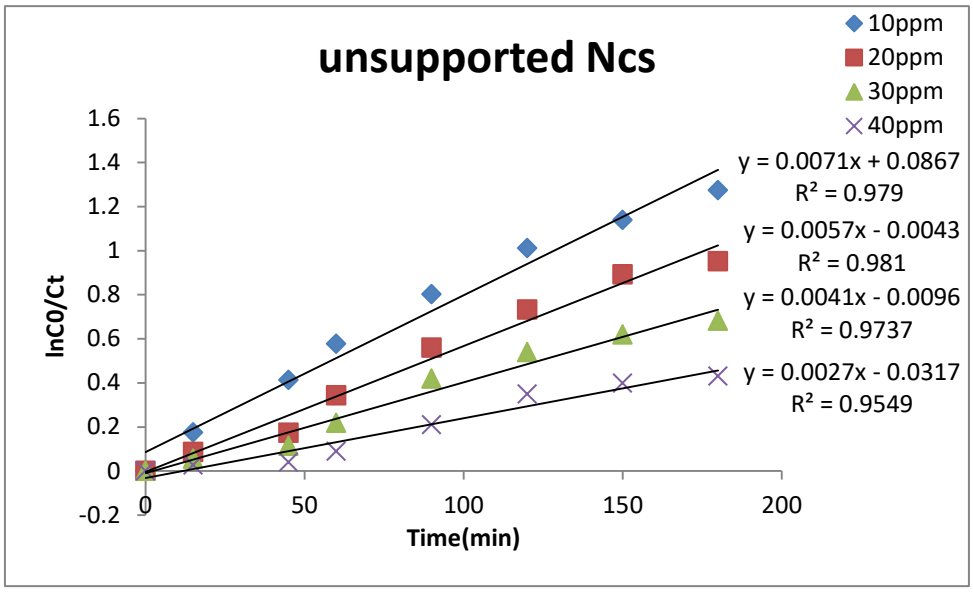

Figure.12. Kinetic effect of ln(Co/Ct) as a function of time for MB degradation at different initial dye concentration of 10, 20, 30 and 40 mg/L with 120mg of unsupported NCS

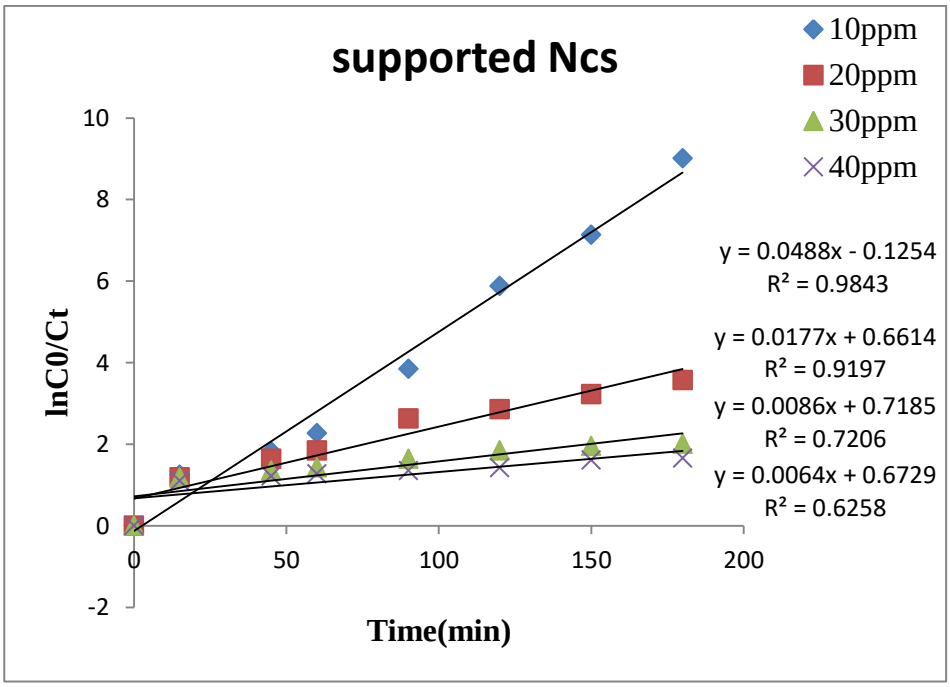

Figure.13. kinetic effect of Z50Ncs (supported Ncs) Plots of ln(Co/Ct) as a function of time for MB degradation at different initial dye concentration of 10, 20, 30 and 40 mg/L, respectively.

This pseudo-first order kinetics of the MB degradation process under visible light irradiation may be related to the existence of non-saturated active sites of the photocatalyst (Kajdas, C *et al*..2010).

5. SUMMARY AND CONCLUSIONS

Unsupported and supported Cu_2O-Ag_3PO_4-ZnO composites were synthesized by precipitation method. A facile and convenient method to prepare nanoparticles was chemical precipitation technique. Two or more soluble salts solutions were mixed in a definite ratio and co-precipitated with a base solution under inert atmosphere. By using, 0.1M solutions of $CuCl_2 \cdot 2H_2O$, zinc nitrate hexahydrate (Zn $(NO_3)_2.6H_2O$), $AgNO_3$ and Na_2HPO_4 as precursors with aqueous solutions, however zeolite supported Cu_2O-Ag_3PO_4-ZnO fine particles was prepared by solid state reaction of the as synthesized nanocomposite with natural zeolite. The crystal structures and compositeswere studied using XRD and the photocatalytic activities of all sample, ternary nanocomposite and Zeolite nanocomposite using initial MB concentrations were evaluated under visible light. The degradation process was monitored by an UV–vis absorbance spectrometer (measuring the absorbance of MB at 664 nm). The degradation of the MB was calculated according to the initial and final absorbance of MB in the solutions. The photocatalytic degradation efficiency of the supported composite is higher than unsupported photocatalyst under visible light irradiation for 180 min. The maximum degradation efficiency of 88.2% was Z50-Ncs under visible light. Therefore, the active sites exposed for photocatalytic reaction increases as the surface area increases. According to first order reaction kinetics ln(Co/Ct) = kt, values of ln(Co/Ct) as a function of irradiation time, the linear correlation of the plot suggested that, photocatalitic degradation of MB was pseudo first order kinetics. Dyes are extensively used in textile, leather, newsprint recycling and the dye-house wastewater usually comprises various dyes, which are toxic and harmful for both human and aquatic lives.

In this study, we have tried to provide a list of recent immobilized photocatalyst systems (both unseported and supported NCs) that can be investigated as newer alternatives in the realm of immobilized photocatalysts for the pollution remediation. Various important features of photocatalysts immobilised on supports and their efficiency in degrading dyes have been discussed in this review. These type of immobilised catalysts can help in reducing a great stress on environment due to toxic effluents from industries and harmful organic compound.

6. REFERENCES

Ahmad, B.M., Tay, M.Y., Shameli, K., Hussein, M.Z., Lim, J.J., 2011.Green synthesis and characterization Of silver/chitosan/polyethylene glycol nanocomposites without any reducing agent. *International Journal of Molecular Science,* 12: 4872–4884.

Ahmed, S., M.G. Rasu., Wayde, N., Martens, R. Brown and M.A, Hashib. 2010. Heterogeneous photocatalytic degradation of phenols in wastewater: A review on current status and developments. *Journal of Colloid and Interface Science,* 261: 3-18.

Anandan, S. and M, Yoon. 2003. Photocatalytic activites of the nanosized TiO_2 supported Y-zeolites. *Journal of Photochemical Resourece.* 4: 500-632.

Ansari, S.A., Khan, M.M., Ansari, M.O., Lee, J. and Cho, M.H. 2013. Enhanced photocatalytic and photoelectron chemical activity in the ternary hybrid of $CdS/TiO_2/WO_3$ through the cascade electron transfer. *Journal of Physical Chemistry*. 117: 27023–27030.

Bamba, D., Atheba, P., Robert, D., Trokourey, A., Dongui, B., 2008. Photocatalytic degradation of the diuron pesticide. *Environmental Chemical Engineering,* 6;163-167.

Bouzaza, A., Laplanche, Torimoto., S. Sampath, S. Kuwabata, H.Yoneyama, C. Anderson,A.J. Bard, K. Shimizu, T. Kaneko, T. Fujishima, T. Kodama, H. Yoshida,Y. Kitayama, 2002. Removal of synthetic textile dyes from waste waters. *Journal of Hazardous Materials 141; 520–528*.

Boiarkina, I., Norris, S., Patterson, D.A., 2013. Investigation into the effect of flow structure on the photocatalytic degradation of methylene blue and dehydroabietic acid in a spinning disc reactor. *Journal of Chemical Engineering*. 222; 159-171.

Chan, L., Yang, S., Lixin, C. & Shaowei, C. 2013. TiO_2 nanotubes/ZnO/CdS ternary nanocomposites: preparation, characterization and photocatalysis. *Journal of the Chinese Advanced Materials Society*, 1:3, 188-199.

Chaudhry, Q.S. M., Blackburn, J., Ross, B., Boxall, A. & Castle, L. 2008. Applications of nanotechnologies for the food sector. *Food Additives and Contaminants*. 25(3): 241–258.

Cao, J., B.D, Luo,, H.L, Lin., B, Xu., Chen, S. 2012. Aluminum salt slag characterization and utilization. Review article, *Journal of Hazardous Materials*, 217–218:1-458.

Cao, S., Liu, B., Fan, L., Yue, Z., Liu, B., Cao, B. 2014. Highly antibacterial activity of Ndoped TiO2 thin films coated on stainless steel brackets under visible light irradiation. *Applied Surface Science*. 309; 119-127.

Chen, C.C., Lu, C.S., Chung, Y.C., Jan, J.L., 2007. UV light induced photo degradation of malachite green on TiO2 nanoparticles. *Journal of Hazard. Material*. 141; 520-528.

Chen, C., Ma, W, and Zhao, J. 2010. Semiconductor mediated photodegradation of pollutants under visible-light irradiation. *Chemical Society Revolution* 39(11): 4206-4219.

Chen, C., J. Liu., P. Liu and B. Yu. 2012. Investigation of Photocatalytic Degradation of Methyl Orange by Using Nano-Sized ZnO Catalysts. *Advanced Chemical Engineering Science*. 1: 9-14.

Chen, H.Y., Zahraa, O., Bouchy, M., 1997. Inhibition of the adsorption and photocatalytic degradation of an organic contaminant in an aqueous suspension of TiO_2 by inorganic ions. *Journal of Photochemical and Photobiology Applide Chemistry*. 108; 37-44.

Dong, Y., Liu, Z., Chen, L. 2012. Removal of Zn(II) from aqueous solution by natural hallo site nanotubes. *Journal of Radio anal Nuclar Chemistry.* 292, 435–443.

Exposito, A.J., Patterson, D.A., Mansor, W.S.W., Monteagudo, J.M., Emanuelsson, E., Sanmartín, I., Dur_an, A. 2017. Antipyrine removal by TiO2 photocatalysis based on spinning discreactor technology. *Journal of Environmental Science.* 187; 504-512.

Friedman, H.L, 2009. "Kinetics of thermal degradation of char-forming plastics from thermogravimetry. Application to a phenolic plastic". *Journal of Applied Surface Science.* 6; 183-195.

Gaya, U.I. and Abdullah A.H. 2008. Heterogeneous photocatalytic degradation of organic contaminants over titanium oxide:a review of fundamentals, progress and problem. *Journal of Photochemistry and Photobiology*, 9:112-119.

Heinlaan, M., Ivask, A., Blinova,Ii. and Dubourguier, H.C. 2008. Toxicity of nanosized and bulk ZnO, CuO and TiO_2 to bacteria Vibrio fischeri and crustaceans Daphnia magna and Thamnocephalus platyurus. *Journal of Colloid and Interface Science. 71*: 1308–13017.

Helaïli, N., Bessekhouad, Y., Bouguelia, A. and Trari, M. 2010. P-Cu_2O/n-ZnO heterojunction applied to visible light Orange II degradation. *Journal of Soil Engineering*, 84:1187–1192.

Herrmann, J.-M., Matos, J., Disdier, J., Guillard, C., Laine, J., Malato, S., Blanco, J., 1999. Solar photocatalytic degradation of 4-chlorophenol using the synergistic effect between titania and activated carbon in aqueous suspension. *Catalytic Science and Technology*, 54; 255-265.

Jain, N.; Bhargava, A.; Panwar, J. 2014**.** Enhanced photocatalytic degradation of methylene blue using biologically synthesized "protein-capped" ZnO nanoparticles. *Journal of Chemical Engineering, 243*: 549–555.

Jiang, T., Xie , T., Chen, L. and Wang, Z. 2013. Carrier concentration-dependent electron transfer in Cu_2O/ZnO nanorod arrays and their photocatalytic performance. *Journal of Colloid and Interface Science.* 5: 2938–3944.

Jyoti, P., Borah, J., Barman, K., Sharma, C. 2008. Structural and optical properties of ZnS nanoparticles. *Journal of Colloid and Interface Science*. 5: 201-208.

Kasanen, J., Salstela ,J., Suvanto.M. and T.T. 2011. An efficient visible light sensitized composite with its application in photocatalytic degradation of Rhodamine B. *Applid Surface Science,* 258: 1738–1743.

Kajdas, C., Kulczycki, A., Kurzydlowski, K., Molina, G., 2010. Activation energy of tri biochemical and heterogeneous catalytic reactions, *Applied Surface Science.* 28; 523–533.

Khatamian, M.,. Divband, B., Jodaei, A. 2012. Degradation of 4-nitrophenol (4-NP) 340 using ZnO nanoparticles supported on zeolites and modeling of experimental results by artificial neural networks. *Journal of Physical Chemistry*. 134(1):31–37.

Kikugawa, T., Yi, Z., J.H, G., N, Ye., Kako, S.X., Ouyang, H., Stuart-Williams, H., Yang, J.Y., Cao, W.J., Luo, Z.S., Li, Y., Liu, Withers, R.L. 2010. An orthophosphate semiconductor with photooxidation properties under visible-light irradiation. *Journal of Chemical Education*. 9: 559-564.

Kim, H., Kim, J., Kim, W. and Choi, W. 2011. Enhanced photocatalytic and photoelectrochemical activity in the ternary hybrid of CdS/TiO_2/WO_3 through the cascadal electron transfer. *Journal of Physical Chemistry*, 115: 9797–9805.

Koziej, D., Lauria, A. and Niederberger, M. 2014. 25th anniversary article: metal oxide particles in materials science: addres all length scales. *Catalysis Today*, 26: 235–257.

Krishna, V., Pumprueg, S., Lee, S. H., Zhao, J., Sigmund, W., Koopman, B .and Moudgil, B. M. 2005. Photocatalytic disinfect ion with titanium dioxide coated multi-wall carbon nanotubes. *Process of Safety Environmental Protection.* 83:393–397.

Kumar, S.G., Devi, L.G., 2011. Review on modified TiO2 photocatalysis under UV/visible light: selected results and related mechanisms on interfacial charge carrier transfer dynamics. *Journal of Physical Chemistry*. 115; 13211-1324.

Lanje, A.S., Sharma, S.J.; Ningthoujam, R.S.; Ahn, J.S.; Pode, R.B. 2013. Low temperature dielectric studies of zinc oxide (ZnO) nanoparticles prepared by precipitation method. *Advanced Powder Technology*, 24:331–335.

Liang XD, Gao L, Yang SW, Sun J. 2009. Facile synthesis and shape evolution of single crystal cuprous oxide. *Catalysis Today.* 21:2068-2071.

Liu, H., Yang, J., Zhang Y., Chen, S., Walsh, A.,. Xiang, H.,. Gong, X. and Wei, S. 2013. Prediction Of $(TiO_2)x(Cu_2O)y$ Alloys For Efficient Photoelectron-Chemical Water Splitting. *Journal of Physical Chemistry*. 15: 1778-1789.

Liu, Z., Zhang, X., Nishimoto, S., Jin, M., Tryk, D., Murakami, T. and Fujishima, A. 2008. Highly ordered TiO_2 nanotube arrays with controllable length for photoelectrocatalytic degradation of phenol. *Journal of Physical Chemistry*,112: 253–259.

Mahmoodi, N., Arami, M., Limaee, N. and Tabrizi, N. 2006. Kinetics of heterogeneous photocatalytic degradation of reactive dyes in an immobilized TiO_2 photocatalytic reactor. *Journal of Colloid and Interface Science*, 295:456-462.

Malato, S., Fernandez-Ibanez, P., Maldonado, M.I., Blanco, J., Gernjak, W., 2009. Decontamination and disinfection of water by solar photocatalysis: recent overview and trends. *Catalysis Today*. 147; 1-59.

Malik. P. K. 2003. Use of activated carbons prepared from sawdust and rice-husk for adsorption of acid dyes: a case study of Acid Yellow 36. *Journal of Chemical Education*. 56: 239-249.

Nezamzadeh, Ejhieh,. Banan, Z. 2012. Sunlight assisted photodecolorization of crystal violet catalyzed by CdS nanoparticles embedded on zeolite A. *Desalination, Amsterdam, Volume:* 284:157–166.

Persenaire, O., Alexandre, M., Degee, P., Dubois P.h, 2001. "Mechanisms and kinetics of thermal degradation of poly (epsilon-caprolactone) ". *Biomacro molecules*, 2: 288-294.

Pouretedal, H.R., A.Norozi. MH. Keshavarz and A.Semnani. 2009. Nanoparticles of zinc sulfide doped with Mn, Ni and copper as nanophotocatalyst in the degradation of organic dyes. *Journal of Hazardous Matterials*, 162:674-681.

Rajoriya , R.K., Parasad , B., Mishra, I.M. and Wasewar , K. L. 2011. Adsorption of benzaldehyde on granular activated carbon : Kinetics, equilibrium, and thermodynamic. *Journal of Hazardous Materials*. 196: 109 – 114.

Rajic, N., Stojakovic, D.,Jovanovic, M., Zabukovec Logar, N., Mazaj, M. and Kaucic, V. 2010. Removal of nickel(II) ions from aqueous solutions using the natural clinoptilolite and preparation of nano-NiO on the exhausted clinoptilolite. *Applied Surface Science*, 257:1524–1532.

Rinco´n, A.G., Pulgarin, C., 2005. Use of coaxial photocatalytic reactor (CAPHORE) in the TiO2 photo-assisted treatment of mixed E. coli and Bacillus sp. and bacterial community present in wastewater. *Catalyst Today*, 101; 331-344.

Salinaro, A., 1999. Terminology, relative photonic efficiencies and quantum yields in heterogeneous photocatalysis. Part II: experimental determination of quantum yields. *Pure Applied Chemistry*,10;1351-1020321.

Shen, C.,Wang, Y.J., Xu, J.H., Luo, G.S., 2015. Glass capillaries with TiO2 supported on inner wall as microchannel reactors. *Journal of Chemical Engineering.* 277; 48-55.

Singh, P., Kaur, D., 2010. Room temperature growth of nanocrystalline anatase TiO_2 thin films by dc magnetron sputtering. *Journal of Chemical Education.* 405, 1258-1266.

Solomon, S.D., Bahadory, M., Jeyarajasingam, A.V., Rutkowsky, S.A., 2007. Synthesis and study of silver nanoparticles. *Journal of Chemical Education*, 84:322–329.

Soto K. F., Carrasco A., Powell T. G., Garza K. M., and Murr L. E. 2005. Comparative in vitro toxicity assessment of some manufactured nanoparticulate materials characterized by transmission electron microscopy. *Journal of Pure Applied Chemistry*. 7: 145-169.

Sonawane, R., Hegde, S., Dongare, M., 2003. Preparation of titanium(IV) oxide thin film photocatalyst by solegel dip coating. *Journal of Pure Applied Chemistry*. 77; 744-750.

Stojakovic, D., Hrenovic, J., Mazaj, M. and Rajic, N. 2011. On the zinc sorption by the Serbian natural clinoptilolite and the disinfecting ability and phosphate affinity of the exhausted sorbent. *Journal of Hazards Material*, 185: 408–415.

Tang, E., Cheng, G., Maa, X., Pang, X. and Zhao, Q. 2006. Surface modification of zinc oxide nanoparticle by PMAA and its dispersion in aqueous system. *Applied Surface Science,* 252: 5227–5232.

Ullah R., Dutta. J., 2008. Photocatalytic degradation of organic dyes with manganese doped ZnO nanoparticles. *Journal of Hazardous Material*. 156; 194–200.

Vaiano, V., Sacco, O., Sannino, D., Ciambelli, P., 2015. Nanostructured N-doped TiO_2coated on glass spheres for the photocatalytic removal of organic dyes under UV or visible light irradiation. *Journal of Applied Science.* 170; 153-161.

Wang, S.L., Li, P.G., Zhu, H.W. and Tang, W.H. 2012. Controllable synthesis and photocatalytic property of uniform CuO/Cu_2O composite hollow micro-spheres. *Journal of Hazard Material.* 230:48–53.

Wei, S., Ma, Y., Chen, Y., Liu, L., Liu, Y. and Shao, .Z. 2011. Fabrication of WO_3/ Cu_2O composite films and their photocatalytic activity. *Journal of Hazard Material*, 194: 243–249.

Zahir, M.H., Suzuki, T., Fujishiro, Y.M., Awano, M., 2009. Perovskites with cotton-like morphology consisting of nanoparticles and nanorods: synthesis by the combustion method and their NOx adsorption. *Application of Catalysis.* 361: 86–92.

Zhang , L., Ai, C Liao. F. et al., 2011. " Removal of methylene blue from aqueous solution with magnetite loaded multi – wall carbon nanotube : kinetic , isotherm and mechanism analysis", *Journal of Hazardous Material*. 198: 282 -290.

Zhou, F., Hu, S., Wang, L. and Zhang, J.2011. Preparation of Cu_2O/CeO_2 hetero junction photocatalyst for the degradation of Acid Orange 7 under visible light irradiation. *Catalysis Today.* 12:794–797.

Zhang .D.L. 2007.The research on the production and photocatalysis property of cuprous oxide. . *Application of Catalysis.*03; 121-174.

Zuo, J., 2010. Deposition of Ag nanostructures on TiO2 thin films by RF magnetron sputtering. *Journal of Applied Surface Science*. 256; 7096-7101.

7. APENDICS

7.1.Data Analysis of unsupported Ncs and zeolite supported Ncs.

Appendix Table 1. Percentage degradation of MB as function of time under visible light irradiation by varying the amount of MB solution and keeping unsupported Ncs Ag3PO4-ZnO-Cu2O constant in 180 min.

Time	10ppm	20ppm	30ppm	40ppm
0	0	0	0	0
15	12.3	8.1	5.4	2.6
30	19.5	11.9	7.5	2.9
45	34.2	16.4	12.1	3.9
60	43.6	28.8	19.6	8.4
75	55.4	37.4	26.7	13.5
90	61.7	43.1	34.2	18.9
105	66.1	49.2	39.6	24.5
120	69.4	51.5	41.7	29.4
135	71.7	55.7	44.6	31.9
150	71.8	59.4	46.2	32.8
165	71.8	60.2	48.5	34.6
180	72.82	61.3	49.4	35.2

Appendix Table 2. Percentage degradation by varying the amount of MB using unsupported Ncs in the form of lnC0/Ct ratio under visible rad.

Time	10ppm	20ppm	30ppm	40ppm
0	1	1	1	1
15	0.174	0.086	0.055	0.026
30	0.223	0.131	0.079	0.03
45	0.412	0.173	0.113	0.039
60	0.577	0.343	0.218	0.088

75	0.819	0.464	0.311	0.124
90	0.967	0.559	0.418	0.209
105	1.169	0.713	0.504	0.281
120	1.203	0.732	0.538	0.349
135	1.272	0.819	0.59	0.384
150	1.273	0.891	0.619	0.397
165	1.274	0.94	0.665	0.424
180	1.274	0.951	0.681	0.43

Appendix Table 3. Percentage degradation of MB as function of time under visible light irradiation by varying the amount of MB solution and keeping supported Ncs Ag_3PO_4-ZnO-Cu_2O constant in 180 min.

Time	10ppm	20ppm	30ppm	40ppm
0	0	0	0	0
15	19.3	16	14.7	9.4
30	26.9	25.2	17.5	14.7
45	44.2	38.7	26.2	17.5
60	56.3	45.3	29.7	21.1
75	68.4	59.5	36.5	24.4
90	73.1	62	38.9	25.2
105	79.3	62.9	41.4	26.8
120	82.5	64.8	45.8	29.4
135	84.2	65.3	47.2	34.7
150	86.1	68.5	48.6	37.3
165	87.5	69.7	49.2	38.9
180	88.2	71.5	50.1	39.6

Appendix Table 4. Percentage degradation by varying the amount MB using supported Ncs in the form of lnC0/Ct ratio under visible rad.

Time	10ppm	20ppm	30ppm	40ppm

0	0	0	0	0
15	1.25	1.19	1.18	1.1
45	1.82	1.64	1.35	1.22
60	2.27	1.85	1.43	1.27
90	3.85	2.63	1.64	1.35
120	5.88	2.86	1.85	1.42
150	7.14	3.23	1.96	1.61
180	9.01	3.57	2.01	1.66

Appendix Table. 5. % degradation of MB (10ppm) as function of time under visible light with unsupported Ncs and supported Ncs of Ag_3PO_4-ZnO-Cu_2O in 180 min.

Time	Ncs	Z-50	Z-35Ncs
0	0	0	0
15	12.3	19.3	16.2
30	19.5	26.9	21.4
45	34.2	44.2	37.3
60	43.6	56.3	49.8
75	55.4	68.4	66.3
90	61.7	73.1	69.7
105	66.1	79.3	74.5
120	69.4	82.5	76.1
135	71.7	84.2	79.6
150	71.8	86.1	81.9
165	71.8	87.5	83.7
180	72.82	88.2	84.5